Fragmentation and migration of invasion percolation clusters: Experiments and simulations

G. Wagner, A. Birovljev, P. Meakin, J. Feder, and T. Jøssang
Department of Physics, University of Oslo, Box 1048, Blindern, 0316 Oslo 3, Norway
(Received 12 August 1996; revised manuscript received 6 February 1997)

Experimental studies of two fluid displacement processes in porous media involving extensive fragmentation of invasion percolationlike structures are described. In the first process, a two-dimensional porous cell saturated with a wetting fluid was slowly invaded by air. The air formed a fractal structure that fragmented when the pressure of the wetting fluid increased and the air was driven out of the system. In the second process, a fractal air structure migrated through a two-dimensional porous medium saturated with wetting fluid. The structure was driven by increasing buoyancy forces and fragmented. The fragments migrated, fragmented, and coalesced with other fragments. The processes were simulated using new site-bond invasion percolation models that captured the displacement mechanisms and reproduced the fragmentation events, and good agreement was found. In both processes, the fractal dimensionality of the fragments was equal to the dimensionality $D \approx 1.82$ of the initial invasion percolationlike structures. The fragment size distributions measured in both processes and the dynamics of the migration process could be described by simple scaling forms.
[S1063-651X(97)11906-7]

PACS number(s): 47.55.Kf, 47.55.Mh, 05.40.+j

I. INTRODUCTION

Immiscible fluid-fluid displacement processes in porous media lead to the formation of complex, disorderly interfaces that often appear to have a fractal geometry [1]. For instance, when a nonwetting fluid is slowly injected into a two-dimensional porous medium that is saturated with a wetting fluid, the nonwetting fluid forms a fractal structure with a dimensionality of $D \approx 1.82$ [2]. Concepts and models related to percolation theory [3] have been used extensively to study this and other multiphase flow phenomena in the past 20 years [4–9].

The purpose here is to focus on two displacement processes in which the invasion of nonwetting fluid is an initial step. In the first experiment, a fractal nonwetting fluid ''cluster'' is formed by slowly displacing a wetting fluid out of a horizontal two-dimensional porous medium. The injection of nonwetting fluid is stopped when the cluster has reached a given size, and the process is reversed by sucking the nonwetting fluid out of the medium [10]. In the second process, a fractal cluster of nonwetting fluid is formed in the same manner, by slowly displacing wetting fluid out of a porous medium. Then, a hydrostatic pressure gradient is imposed on the system by slowly rotating the two-dimensional medium out of the horizontal plane. Driven by increasing buoyancy forces, the cluster of nonwetting fluid starts to migrate through the medium [11]. In both processes, the initial fractal cluster of nonwetting fluid is found to fragment into smaller pieces. Here we show that the fragments can be described by the same fractal dimensionality as the initial cluster, and that the distribution of fragment sizes can be represented by simple scaling forms.

The initial fractal clusters of nonwetting fluid can be described by a branch of percolation theory known as ''invasion percolation'' [12]. Numerical studies of the fragmentation of percolation clusters have been carried out relatively recently [13–15]. These studies were motivated by the hope of advancing the understanding of the properties of percolation clusters. In this work, a similar hope, and the prospect of applications in areas such as secondary oil migration, has led to the development of new numerical models based on the invasion percolation algorithm [12]. These models include mechanisms for the fragmentation of the nonwetting fluid, and they are able to reproduce the experimental patterns in a satisfactory manner.

The remainder of the paper is organized as follows. In Sec. II, the experimental procedures are described, and displacement patterns observed in the experiments are presented. In Sec. III, the models used to simulate the displacement processes are described, and simulated displacement patterns are presented. In Sec. IV, the distributions of fragment sizes measured in the experiments and in the simulations are compared. In Sec. V attempts to represent the fragment size distributions obtained from simulations by simple scaling forms are described. Conclusions from the work are presented in Sec. VI.

II. EXPERIMENTS

The experimental two-dimensional media consisted of a confined monolayer of 1 mm or 2 mm diameter glass beads. The beads were randomly thrown onto a sheet of sticky contact paper with a rectangular, nonsticky, silicone border until no place for more beads was left. After removal of the excess beads that had not stuck to the contact paper, another sheet of contact paper was applied on top making the model airtight. The two-dimensional bead model was sandwiched between two 25 mm thick polymethylmethacrylate sheets. The lower sheet had a transparent membrane attached to it which, when inflated, pressed the beads against the other sheet to ensure that the cell was only one bead thick everywhere. The pore space formed in this manner had a random geometry. The pores varied in diameter from ≈ 0.5 to ≈ 2 mm and had 3–6 pore necks adjacent to them.

In all the experiments, air was used as the nonwetting fluid. A glycerin-water mixture with 1% Nigrosin black dye

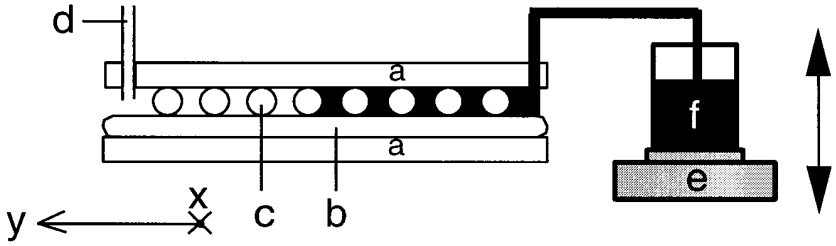

FIG. 1. The experimental setup used in the experiments on IP cluster fragmentation. (a) Supporting plates, (b) inflated membrane, (c) bead layer, (d) inlet for the nonwetting fluid, (e) weight balance, and (f) wetting fluid reservoir. The coordinate system is indicated.

was used as the wetting fluid with respect to air at both the contact paper and glass bead surfaces. This fluid has a viscosity of $\mu = 6 \times 10^{-2}$ P, a density of $\rho = 1123$ kg/m^3, and a surface tension of $\sigma = 44 \times 10^{-3}$ N/m.

A. Experiments on IP cluster fragmentation

The cell was positioned horizontally, evacuated, and saturated with the wetting fluid. The shorter edge of the cell contained an open channel, which served as an inlet. A corresponding channel along the opposite edge was used as an outlet. A reservoir with a glycerine-water mixture was placed on a Mettler PE3600 weight balance. The weight balance rested on a stand with an adjustable height. The liquid in the reservoir was connected to the outlet of the porous medium. The pressure difference $\Delta P = P - P_0$ between the pressure P of the wetting fluid and the atmospheric pressure P_0 was controlled by adjusting the height of the reservoir. The mass of liquid that entered or exited the reservoir was measured by the weight balance. Figure 1 shows the setup.

In the beginning of the experiment the pressure of the wetting fluid was slightly higher than the atmospheric pressure ($\Delta P > 0$). The experiment started by slowly lowering the reservoir with a constant speed $v = 0.5$ cm/h, to continuously reduce ΔP. Wetting fluid was slowly withdrawing from the medium through the outlet, while air entered at the inlet edge and formed an invasion percolationlike displacement pattern. Some regions of wetting fluid became engulfed and isolated from the reservoir by the invading air.

Shortly before the breakthrough of the growing cluster, ΔP had been reduced to a value of ≈ -200 Pa. At this stage, the process was reversed. The reservoir was lifted at a constant speed v. When ΔP increased, the air was driven back. At first, the reservoir was below the plane of the cell ($\Delta P < 0$), to counteract the capillary forces. Further pores were abandoned by the air when the reservoir was lifted above the plane of the cell and ΔP was increased to a final value of ≈ 250 Pa. The invading wetting fluid bypassed some of the receding air and occasionally caused fragmentation of the air cluster. Large regions of the air could become isolated when withdrawal of air from a pore in the vicinity of the air inlet isolated them from the inlet. These cluster fragments remained immobile and could not be displaced by the imbibing wetting fluid. The experiment was terminated when all the remaining air was completely cut off from the edge of the model through which it had entered, and an increase of ΔP did not lead to further displacement.

Figure 2 shows a sequence of displacement patterns observed at breakthrough after air invasion, [Fig. 2(a)], during the withdrawal of air [Fig. 2(b)], and at the final stage at which no more displacement of air was possible [Fig. 2(c)]. At the final stage shown in Fig. 2(c), the remaining air was disconnected from the outlet. The two-dimensional porous media used in the experiment shown in Fig. 2 had a size of $\approx 100 \times 200$ pores. By the end of this experiment, about 35%

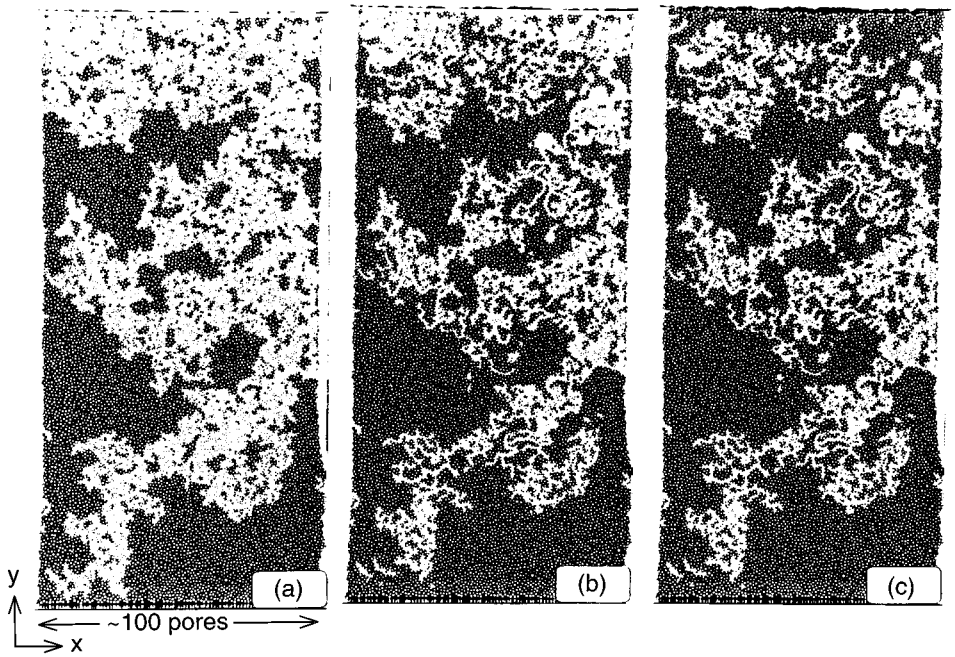

FIG. 2. Patterns observed in a IP cluster fragmentation experiment. Part (a) shows the system at breakthrough. The nonwetting fluid (air, white) had invaded along the top edge in the figure (the cell was horizontal) and displaced part of the wetting fluid (water-glycerol, black) out of the porous medium. The nonwetting fluid formed a connected IP-like cluster. The saturation was $\Gamma \approx 0.37$. (b) The system during the displacement of the nonwetting fluid by the wetting fluid. (c) The remaining cluster fragments that were isolated at the final stage at which no more displacement of nonwetting fluid was possible. The saturation was $\Gamma \approx 0.24$.

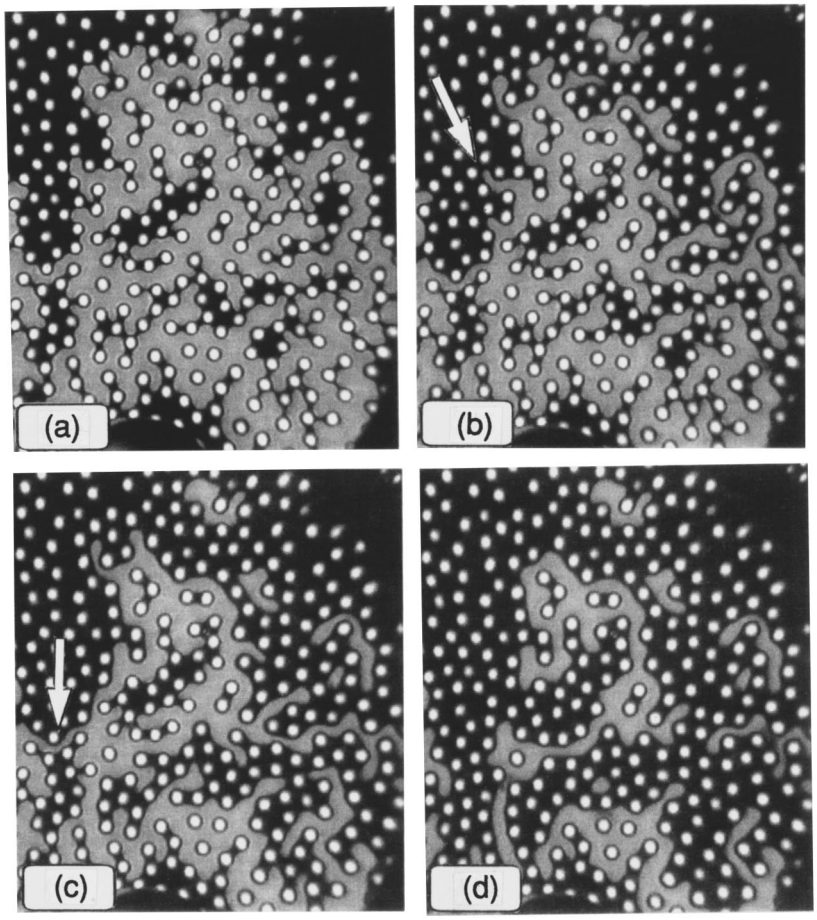

FIG. 3. Close-up images of patterns observed at several stages in a IP cluster fragmentation experiment using point injection. Here the air (light gray) is being forced out of the porous medium by increasing the pressure in the wetting fluid (black). The bright spots indicate the glass beads of the cell. (a) The cluster formed at the end of the invasion of nonwetting fluid. (b) The tips of the cluster receded. (c) Cluster fragmentation took place. (d) Further receding and fragmenting of the tips of the cluster.

of the air contained in the initial cluster was displaced from the cell.

Figure 3 shows a close-up part of an air cluster observed in an experiment in which the air entered and left the cell through a hole in the center of the upper plate. Only a few experiments of this type were carried out, since the withdrawal of nonwetting fluid could come to an early end when the center region became disconnected from the remaining nonwetting fluid cluster. The cluster of nonwetting fluid formed by the invading air was interspersed by thin ''fjords'' of wetting fluid that separated pairs of adjacent invaded pores [Fig. 3(a)]. The fjords consisted of chains of pore necks in which the invading air did not manage to break through [16]. Thus, almost every invaded pore had at least one adjacent pore neck that was filled with wetting fluid but not necessarily connected to the reservoir other than through the wetting films along the edges and hollow spaces of the medium [17].

When the pressure in the wetting fluid increased, the branches of the air cluster became thinner, and the cluster tips retracted [Fig. 3(b)]. At higher wetting fluid pressures, fragmentation could occur, mostly at locations where a channel of air was strongly curved [Fig. 3(c)]. Once a fragment was disconnected, further retraction of tips occurred at other parts of the cluster [Fig. 3(d)]. The sequence of pores from which the air was displaced was different from the sequence of pores invaded during the preceding air invasion process. Retraction of cluster tips often occurred simultaneously in different regions.

The saturation Γ of the experimental cell with nonwetting fluid in an edge-injection experiment increased steeply as the pressure difference ΔP was reduced. The increase is well known from pressure-saturation experiments [18–20] and may be interpreted as a percolation phenomenon [4–6]. As ΔP was increased again after the initial stage in which ΔP was continuously decreased, the saturation Γ decreased and reached a final value at about two-thirds of the breakthrough value.

B. Experiments on IP cluster migration and fragmentation

In these experiments, the cell was placed in a frame that allowed the inclination angle α between the plane of the cell and the horizontal plane to be controlled. The effective acceleration due to gravity acting on the cell was $g \sin(\alpha)$. Figure 4 shows the setup. The cell was evacuated and saturated with the wetting fluid. The cell was positioned horizontally ($\alpha = 0°$), and air was injected slowly through an inlet in the middle of the cell. The displaced wetting fluid exited the cell through outlets at the edges of the cell. In this way an invasion percolationlike cluster of nonwetting fluid was formed.

When the cluster had filled a sufficiently large number of pores ($\approx$2000 to $\approx$10,000 pores), the injection of air was stopped and the cell was sealed. An increasing pressure gradient was imposed by rotating the cell slowly about a horizontal axis (the x axis). Since the air is less dense than the wetting fluid, the cluster experienced buoyancy forces in the

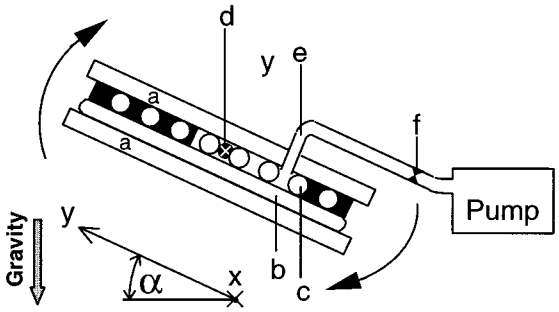

FIG. 4. The experimental setup used in the experiments on IP cluster migration. (a) Supporting plates, (b) inflated membrane, (c) bead layer, (d) rotation axis, (e) inlet for the nonwetting fluid, and (f) valve. The coordinate system and the direction of gravity are indicated.

y direction that competed with the pinning capillary forces. As the inclination angle α was increased, the buoyancy forces overcame the capillary forces and the cluster started to migrate. The migration occurred through a sequence of steps consisting of elementary displacements. The cluster migrated by withdrawing nonwetting fluid from pores at its ''lower'' parts, redistributing it in newly invaded pore spaces at the ''upper'' region of the boundary. An elongated branchlike structure was formed. The branches grew from the upper part of the boundary of the original cluster and meandered in the *y* direction.

As the buoyancy forces increased, the primary branch fragmented and the next generation of small percolationlike air fragments was formed. These fragments became mobilized and started to migrate at larger values of α, later in the experiment. The experiment was terminated when the inclination angle reached its maximum value of $\alpha = 90°$.

The formation of branches increased the extension of the migrating cluster along the direction of the pressure gradient. The buoyancy forces that acted on the cluster were thus increased. At this stage, the cluster was elongated along the direction of the pressure gradient. Eventually, withdrawal events occurred that led to fragmentation of the air cluster. Fragmentation reduced the buoyancy drive, and newly formed fragments were stranded ''behind'' the migrating cluster. When the capillary forces again surpassed the buoyancy forces, the migration of the cluster stopped temporarily. When the inclination angle was further increased, the new fragments started to migrate. Migration was enhanced when fragments moved into contact with each other and coalesced as a result of an increase in the extension in the *y* direction.

Migration and subsequent fragmentation occurred in bursts between long periods of inactivity. The inclination angle α was increased at a constant low rate of 4° per hour so that α could be considered to be constant during migration sequences. The time scale of migration was sufficiently slow to resolve elementary displacement events by eye.

Figure 5 shows a sequence of displacement patterns observed in an experiment using a cell of $\approx 100 \times \approx 200$ pores. Beads with a diameter of 2 mm were used in this experiment. Figure 6 shows a similar sequence using a larger cell and 1 mm beads.

III. SIMULATIONS

The experiments were simulated using stochastic models, based on the invasion percolation algorithm [12]. In the simplest form of IP, an invasion threshold p_i is assigned to each site i on a lattice of sites. The invasion thresholds are random numbers uniformly distributed over the interval 0 to 1. The sites represent pores, and the invasion thresholds represent the sizes of channels that connect the pores. Initially, all the sites are occupied with ''defender'' fluid, and a seed site is then filled with ''invader'' fluid (the label associated with the site is changed from that representing invader fluid to that representing defender fluid). This site represents a growing cluster or region filled by the invader fluid. At each step in the simulation, the site on the unoccupied perimeter of the invader fluid cluster with the lowest threshold is filled. The unoccupied perimeter includes all empty sites that are adja-

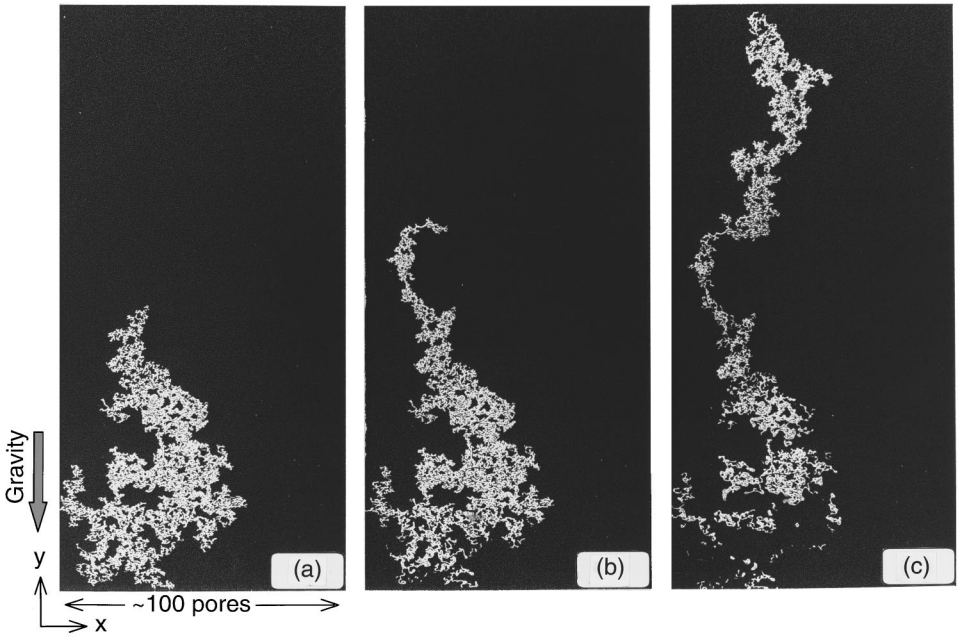

FIG. 5. Three stages in the migration of a IP-like cluster of nonwetting fluid (air, white) covering ≈ 4000 pores through a porous medium saturated with a wetting fluid (water-glycerol, black). The plane of the cell was rotated continuously. The original cluster (a) underwent fragmentation and distortion as the effective acceleration of gravity increased. The photographs were taken at inclination angles of $\alpha = 0°$ (a), 2.1° (b), and 2.4° (c), respectively. The coordinate system and the direction of gravity are indicated.

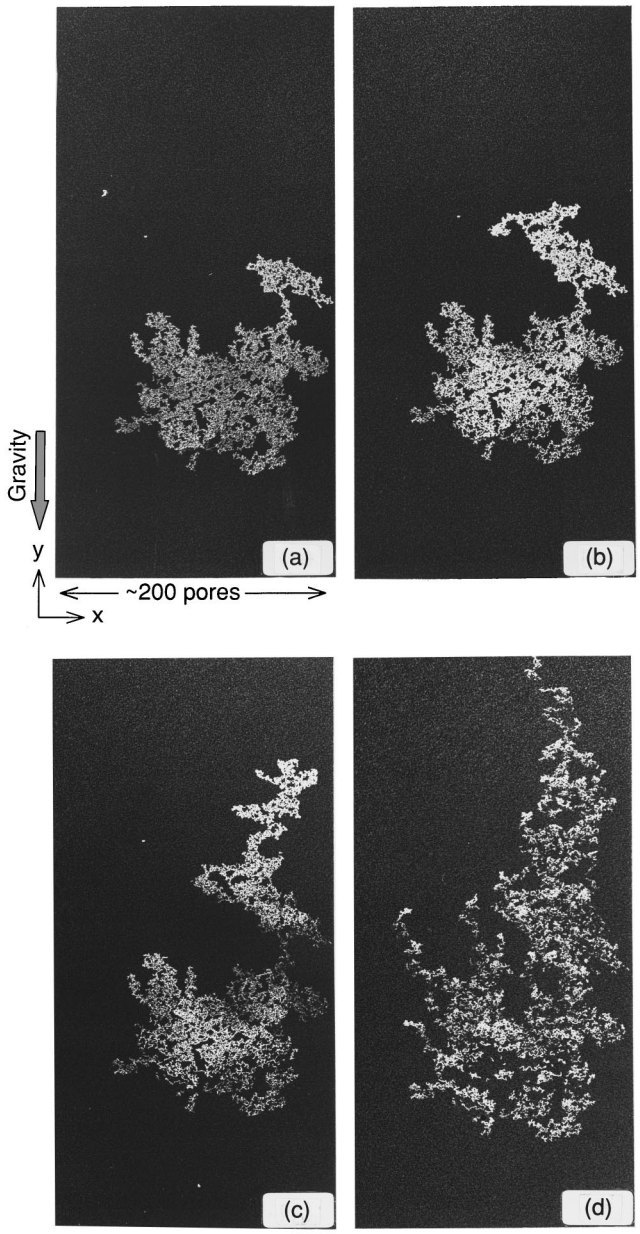

FIG. 6. Four stages in the migration of a IP-like cluster of nonwetting fluid (air, white) covering $\approx 10\,000$ pores through a porous medium saturated with a wetting fluid (water-glycerol, black). The plane of the cell was rotated continuously. The photographs were taken at $\alpha = 0°$ [original cluster, (a)], 2.8° (b), 3.5° (c), and 85.4° (d), respectively. The coordinate system and the direction of gravity are indicated.

cent (nearest neighbors) to filled sites. The filled sites form a fractal cluster embedded in the surrounding defender fluid reservoir.

A. Modeling displacement mechanisms

The mechanisms of slow displacement of wetting fluids by nonwetting fluids in porous media have been studied extensively [17,19–21]. The conclusion from these efforts is that the displacement of a wetting fluid out of a pore and the invasion of the pore by a nonwetting fluid is determined by the geometry of the pore neck that connects the invaded region to the pore. The pressure that the nonwetting fluid must overcome to invade a pore neck is inversely proportional to the size of the neck. The region invaded by the nonwetting fluid has a fractal geometry [2], and the invasion of pores occurs in bursts [22] with a broad, power-law distribution of sizes.

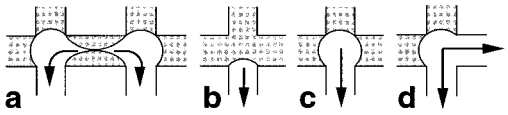

FIG. 7. Schematic illustration of imbibition mechanisms in a square network porous medium. The wetting fluid (shaded) displaces the nonwetting fluid (white). (a) Snap-off invasion of a channel. (b) Pistonlike invasion of a channel. (c) I1 invasion of a pore. (d) I2 invasion of a pore. This figure is taken from Ref. [17].

The opposite process, slow displacement of nonwetting fluid by wetting fluid, is not only governed by the pore size but also by the local configuration of the fluid-fluid interface [19,21,23]. In quasistatic displacements of a nonwetting fluid by a wetting fluid, the channels that connect pores may be invaded by the wetting fluid in ''pistonlike'' processes, or by ''snap-off'' events [17,23] (see Fig. 7). Snap-off invasion occurs at channels that connect two pores filled with nonwetting fluid [Fig. 7(a)]. In narrow channels, the film of wetting fluid that covers the surface of the porous network may swell and eventually choke off the nonwetting fluid [17]. This may separate a connected region of nonwetting fluid into two regions or clusters that are no longer connected. Pistonlike invasion refers to the invasion of a channel at the interface, i.e., one that connects a pore filled with nonwetting fluid with one that is already filled with wetting fluid [Fig. 7(b)].

The nonwetting fluid that occupies pores is preferentially displaced at pores that are connected to the rest of the nonwetting fluid by a single filled channel [''I1 imbibition,'' Fig. 7(c)] [17,23]. If no such pore is available along the interface and the pressure of the invading wetting fluid is sufficiently high, ''I2'' displacements occur [Fig. 7(d)]. I2 refers to the invasion of pores that are connected to the remaining nonwetting fluid by only two filled channels that are adjacent to each other. Other interface configurations have been observed to be of comparable stability.

Although the random geometry of the porous media used in the present work prevented an unambiguous classification, the cluster tip retractions observed [Fig. 3(b)] may be regarded as pistonlike and I1 displacements, respectively. Fragmentation of the structures of air in pores where the fluid-fluid interface was strongly curved may be regarded as I2 and snap-off displacements, respectively. To simulate these processes, a site-bond IP model was used that incorporated the dominant displacement mechanisms I1, I2, piston, and snap-off. The pores in the two-dimensional porous medium were represented as sites on a two-dimensional square lattice and the channels connecting the pores were represented as bonds connecting the sites.

A random number p_i was assigned to each bond i, and a random number q_j was assigned to each site j. The random numbers $\{p\}$ were used to compute the capillary threshold pressure $\phi(q)$ that must be overcome to fill a region with nonwetting fluid. Similarly, the random numbers $\{q\}$ were

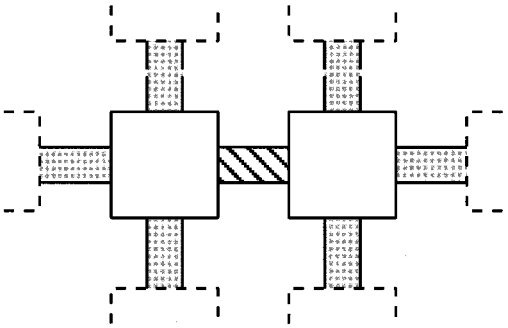

FIG. 8. The six nearest-neighbor bonds of the hatched bond are shaded.

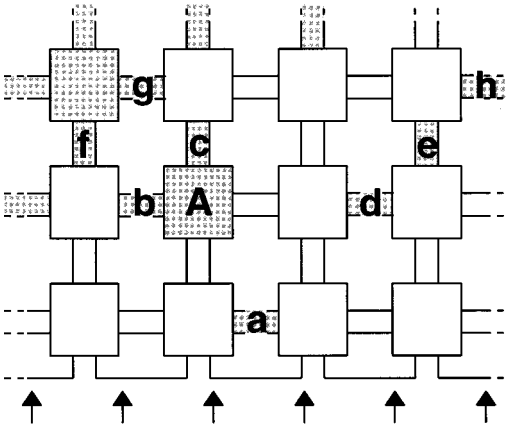

FIG. 9. Illustration of the trapping rules used in the simulations. The simulated nonwetting fluid (white) entered and left the lattice through the inlet row (arrows) and could trap clusters of wetting fluid (shaded). The wetting fluid site A and the bond a are trapped. The wetting fluid bonds $b-e$ are not trapped since they are neighbors to the untrapped wetting fluid bonds f, g, and h, respectively.

used to compute the threshold pressure $\varphi(q)$ required for the simulated nonwetting fluid to withdraw from an invaded region. Infinite invasion thresholds ϕ were assigned to the bonds and sites at the border of the lattice (blocking boundaries).

The distribution of the random numbers $\{p\}$ was selected to represent the distribution of the inverse of the pore neck sizes identified in a digitized image of a section of the experimental cell. The random numbers $\{q\}$ were distributed uniformly on the unit interval.

1. Simulation of the displacement of a wetting fluid by a nonwetting fluid

In the displacement of the simulated wetting fluid by the simulated nonwetting fluid, the invasion threshold ϕ of a bond i was given by $\phi(p_i)=p_i$, and the invasion threshold of a site was zero. In an invasion step, the nonwetting fluid displaced the wetting fluid either from a bond, or from a bond and a site. In each invasion step all of the bonds that were occupied by the wetting fluid and that were adjacent to the region occupied by the nonwetting fluid were identified. The bond with the lowest threshold ϕ was then chosen and ''invaded'' by the nonwetting fluid. If the invaded bond led to a site that was still occupied by the wetting fluid, that site was invaded as well.

To account for the very low compressibility of the displaced wetting fluid, a wetting fluid site was ''trapped'' [12] and could not be invaded by the simulated nonwetting fluid if it was not connected to the surrounding ''infinite'' reservoir of wetting fluid by a path consisting of steps between nearest-neighbor wetting fluid sites. Similarly, a wetting fluid bond was trapped if there was no path consisting of steps between nearest-neighbor wetting fluid sites or wetting fluid bonds leading to the reservoir.

Wetting fluid transport by film flow along the hollow spaces of the cell [17] was included in the simulation in the following manner. The six nearest-neighbor bonds of a bond (see Fig. 8) could connect the wetting fluid in a given bond with the ''infinite'' reservoir of wetting fluid. Collinear bonds could form a connected path of nearest-neighbor wetting fluid bonds even if the sites adjacent to the bonds were filled with nonwetting fluid. In this way, ''fjords'' consisting of bonds occupied with wetting fluid could penetrate the IP cluster of nonwetting fluid, as observed in the experiment [Fig. 3(a)]. Figure 9 illustrates the trapping rules.

2. Simulation of the displacement of a nonwetting fluid by a wetting fluid

In the simulations of the displacement of a nonwetting fluid by a wetting fluid, the four dominant mechanisms (piston, snap-off, I1, and I2 displacement) were included in the model. In a displacement step, the wetting fluid displaced the nonwetting fluid either from a bond (by pistonlike or snap-off processes), or from a site (by I1 or I2 processes). In each step, all the bonds and sites from which the simulated nonwetting fluid could withdraw were identified. The bond or site with the lowest withdrawal threshold φ was chosen, and the nonwetting fluid was withdrawn. This established a hierarchy between the four imbibition mechanisms included in the model [24]. The withdrawal threshold φ assigned to a given bond or site varied according to the local configuration of the fluid-fluid interface.

Table I gives an overview over the assignment of the withdrawal thresholds φ. Nonwetting fluid in bonds that connected a wetting fluid site with a nonwetting fluid site was withdrawn via a pistonlike process. These bonds had a constant minimal withdrawal threshold of $\varphi=-1$. Fluid in bonds that connected two nonwetting fluid sites was withdrawn by snap-off. These bonds had a constant maximal withdrawal threshold of $\varphi=0$. Nonwetting fluid at sites with a single adjacent nonwetting fluid bond was withdrawn via the I1 mechanism. These sites had a low withdrawal threshold of $\varphi(q)=-(q+1)/2$ (depending on the random numbers $\{q\}$ assigned to the sites). Finally, fluid at sites with two

TABLE I. Assignment of withdrawal thresholds φ used in the simulation of the displacement of nonwetting fluid by wetting fluid.

Mechanism	φ
Pistonlike bond withdrawal	$\varphi=-1$
Type-I1 site withdrawal	$-1\leqslant\varphi\leqslant-0.5$
Type-I2 site withdrawal	$-0.5\leqslant\varphi\leqslant0$
Snap-off bond withdrawal	$\varphi=0$

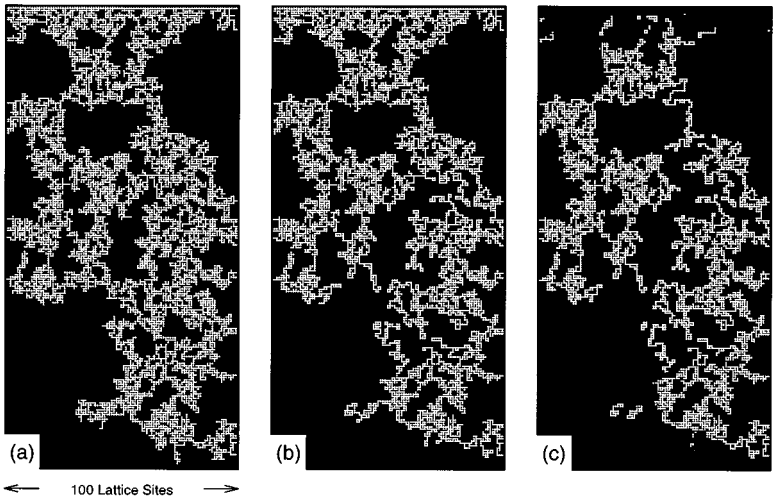

FIG. 10. Patterns obtained during the simulation of IP cluster fragmentation experiments. (a) IP cluster of nonwetting fluid (white) formed at the end of the displacement of wetting fluid by nonwetting fluid (breakthrough). The nonwetting fluid entered along the top, and 6995 sites had been invaded ($\Gamma = 0.35$). (b) The system during displacement of nonwetting fluid by wetting fluid at a wetting fluid ''pressure'' of $-1/2$. At this stage, no I2 withdrawals had occurred, and 6139 sites were invaded ($\Gamma = 0.31$). (c) The system at the final stage when no more withdrawal was possible. 4898 sites remained invaded ($\Gamma = 0.24$).

adjacent nonwetting fluid bonds forming a right angle was withdrawn by the I2 process, using a higher (less negative) random withdrawal threshold of $\varphi(q) = -q/2$. Nonwetting fluid at sites with all other configurations of adjacent bonds could not be withdrawn.

To satisfy the condition of incompressibility of the wetting fluid, only nonwetting fluid at sites that were adjacent to untrapped wetting fluid sites (connected to the surrounding reservoir of wetting fluid by a path consisting of steps between nearest-neighbor wetting fluid sites) could be withdrawn. Similarly, bond withdrawal was only possible for bonds with untrapped wetting fluid bonds among their nearest-neighbor bonds (see Fig. 8). When applying the trapping rules, the sites and bonds forming the blocking boundary were counted as nonwetting fluid sites and bonds.

B. Simulation of the experiments on IP cluster fragmentation

To simulate the displacement experiments described in Sec. II A, one of the shorter edges of a lattice of size $L \times 2L$ represented the injection edge for the nonwetting fluid, and the opposite edge represented the ''infinite'' reservoir of wetting fluid. The sites along the longer edges were blocked to represent the impenetrable walls of the cell.

The simulations began by labeling the row of sites and bonds along one edge of length L to represent nonwetting fluid at the injection edge. The remaining sites and bonds were labeled to represent the wetting fluid. An IP cluster of nonwetting fluid was formed by carrying out a series of invasion steps with trapping, as described in Sec. III A 1. The invasion of nonwetting fluid was terminated at breakthrough when the IP cluster extended along the entire lattice and reached the edge representing the reservoir of wetting fluid.

In the second part of the simulations, the withdrawal of the simulated nonwetting fluid and the invasion of the wetting fluid was simulated by withdrawing nonwetting fluid bonds and sites from the lattice, in the manner described in Sec. III A 2. The withdrawals represented transport through the inlet (the former injection edge at the edge of the lattice).

Fluid from nonwetting fluid sites and bonds was withdrawn in the order of the withdrawal thresholds φ assigned to the corresponding bonds and sites. In a typical sequence of withdrawals, bond and site withdrawals by piston and by I1 steps occurred until no more nonwetting fluid at sites with three adjacent wetting fluid bonds was present, and no more piston or I1 steps were possible. Then a site withdrawal by an I2 step occurred. This always enabled a new series of I1 and piston withdrawal steps to take place. Snap-off withdrawals of fluid from bonds occurred only at the final stage of the simulation due to the high withdrawal threshold assigned to this process.

Some of the withdrawals of nonwetting fluid sites and bonds caused fragmentation of the original IP cluster formed during the invasion of nonwetting fluid. Fluid at sites and bonds that were disconnected from the inlet (because no path consisting of steps between nearest-neighbor nonwetting fluid sites and bonds to the inlet existed) could not be withdrawn anymore. These bonds and sites formed immobile fragments of the original IP cluster.

Figure 10 shows a typical sequence of displacement patterns obtained during a simulation on a lattice of size 100×200. The initial IP cluster of nonwetting fluid occupied 6995 sites. The simulation of the subsequent displacement of the nonwetting fluid by the wetting fluid led to the withdrawal of about 30% of the nonwetting fluid. Right after the beginning [Fig. 10(a)], all nonwetting fluid bonds that had untrapped wetting fluid bonds among their neighbor bonds and that connected a nonwetting fluid site with a wetting fluid site were withdrawn via pistonlike processes. While the ''pressure'' of the wetting fluid, represented by the maximum withdrawal threshold of the bonds and sites that had been withdrawn at each stage, increased from -1 to $-1/2$, I1 withdrawal steps occurred [Fig. 10(b)].

When the ''pressure'' of the invading wetting fluid increased further, I2 withdrawal became possible. These steps could lead to fragmentation of the IP cluster. Most of the I2 withdrawal steps turned one or more adjacent nonwetting fluid sites into ''dangling ends'' that had only a single adjacent bond connecting them to the IP cluster, and that then could be withdrawn in an I1 step. I2 withdrawal steps could also reconnect trapped clusters of wetting fluid to the wetting fluid reservoir. These clusters were then not trapped anymore, and the nonwetting fluid sites adjacent to these clusters became exposed to withdrawal too.

When the wetting fluid ''pressure'' reached the final value of 0, nonwetting fluid bonds that were still connected to the

inlet row were withdrawn by snap-off. Each such withdrawal could enable further site withdrawals since it exposed additional sites to I1 or I2 withdrawal. In the final stage shown in Fig. 10(c), the remaining nonwetting fluid was split up in several clusters (some of them only separated by a bond occupied with wetting fluid). A small fraction of wetting fluid was still trapped.

C. Simulation of the experiments on IP cluster migration and fragmentation

To represent the displacement experiments described in Sec. II.B., the injection of nonwetting fluid into the experimental cell at an inclination angle $\alpha = 0°$ was simulated, using a lattice of lattice of size $L \times 2L$. An injection site in the center of the lattice was labeled to represent nonwetting fluid. The remaining sites and bonds were labeled to represent wetting fluid. An IP cluster was grown by filling bonds and sites adjacent to the nonwetting fluid region with nonwetting fluid, in the manner described above. The invasion was terminated when the cluster had reached a given size.

At this stage, the migration of the IP cluster, under the influence of increasing buoyancy forces, was simulated. The simulation consisted of a sequence of migration steps that involved either the migration of a bond, the migration of a site, or the simultaneous migration of a site and an adjacent bond. In each step, nonwetting fluid was withdrawn from a source site (bond), and migrated by invading a destination site (bond). The numbers of nonwetting fluid bonds and sites were conserved separately.

The migration steps were driven by buoyancy, expressed as the product of a parameter f times the distance along the y-axis between the source and the destination, and opposed by capillary forces. The buoyancy parameter f represented the effective buoyancy force per unit volume $\Delta\rho g \sin\alpha$ in the experiment, where $\Delta\rho$ is the density difference between the wetting and the nonwetting fluid. At each stage, the pressure balance

$$\Pi = \phi + \varphi - f\Delta y \tag{1}$$

was evaluated for all possible migration steps, and the step yielding the minimum balance Π_m was determined. The first two terms on the right-hand side of Eq. (1) represent the capillary forces required for the nonwetting fluid to invade the destination site (bond) and to withdraw from the source site (bond). The framework of invasion thresholds ϕ and withdrawal thresholds φ described above was used. Since the withdrawal thresholds φ were negative, a migration step was supported by the contribution of the capillary force controlling the withdrawal of the nonwetting fluid from a source site (bond). The last term in Eq. (1) accounts for the driving buoyancy force determined by the height difference Δy between source and destination and the buoyancy parameter f.

The migration step yielding a minimum balance Π_m was carried out if $\Pi_m < 0$ and $\Delta y > 0$. The first condition was met if the threshold ϕ assigned to a step was low or if the threshold φ and the height difference Δy between source and destination were large. The second condition was necessary to avoid unphysical loops with nonwetting fluid migrating back and forth. If no migration step was possible, the buoyancy parameter f was increased in small steps.

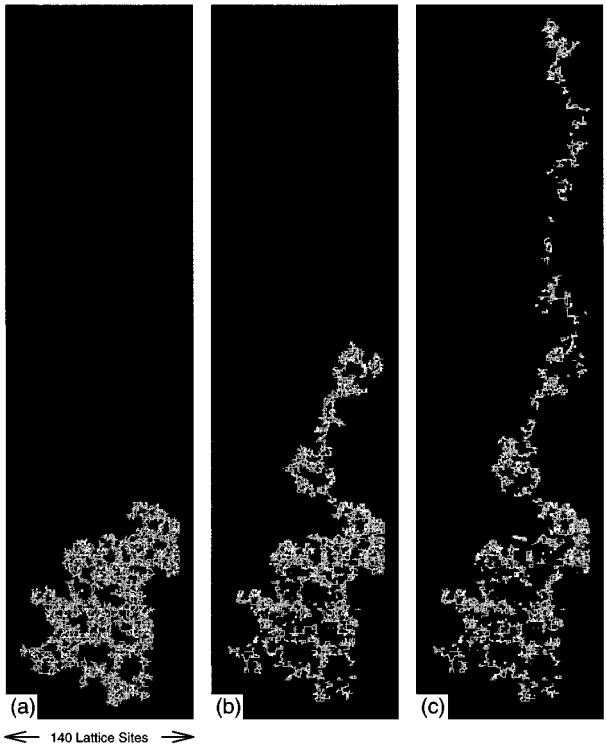

FIG. 11. Patterns obtained during the simulation of IP cluster migration experiments. (a) The system at the end of the simulation of invasion of nonwetting fluid (white). An IP cluster covering 6000 sites was formed. (b) A meandering branch grew at $f = 0.0036$. (c) The nonwetting fluid cluster was highly fragmented at $f = 0.0106$.

Some of the migration steps involving withdrawals by I2 steps or by snap-off processes led to fragmentation of the migrating IP cluster. The fragments migrated independently from each other and could coalesce. The destination site (bond) and the source site (bond) in a migration step had to be part of the same fragment of nonwetting fluid.

In each migration step, incompressibility of the wetting fluid was taken into account. Clusters of wetting fluid that became engulfed by migrating nonwetting fluid were trapped. Migration steps were only possible if both the destination site (bond) and source site (bond) were adjacent to the same cluster of wetting fluid (including the surrounding ''infinite'' cluster). The withdrawal of nonwetting fluid frequently led to reconnection of trapped clusters of wetting fluid with the surrounding ''infinite'' cluster of wetting fluid.

The migration of the nonwetting fluid fragments occurred in bursts, similarly to those observed in the experiments. After a fragment had started to migrate, a multitude of migration steps took place. The extension of the migrating fragment in the y direction was reduced by repeated fragmentation events. When the buoyancy drive became too weak to support further migration of the fragment, the migration ceased. When the buoyancy parameter had increased significantly, the fragment could migrate further. Coalescence with other fragments increased the y extension and prolonged migration. Figure 11 shows a sequence of displacement patterns

obtained in a simulation in which f was increased in steps of size 10^{-4} from 0 to 0.01.

D. Modifications and simplifications of the simulation models

In some simulations of the cluster fragmentation experiment (Sec. II A.), the distinction between I1 and I2 site withdrawal processes was dropped. For both I1 and I1 site withdrawals, the withdrawal thresholds φ were given by $\varphi(q)=-q$, rather than by using the scheme described in Sec. III A 2. In the absence of a bias in favor of I1 site withdrawal, a smaller amount of nonwetting fluid was displaced. Nonwetting fluid was withdrawn from sites at all parts of the IP cluster since the enhanced withdrawal of sites with two adjacent neighbor bonds opened ''channels'' for the displacing wetting fluid. The regions of wetting fluid close to the outlet became untrapped at an early stage. This enabled withdrawal of nonwetting fluid that was located near the outlet. Large fractions of the IP cluster became disconnected and could not be withdrawn.

In another variant of the model, the threshold for bond snap-off was not constrained to the value $\varphi=0$. At the beginning of a simulation of cluster fragmentation, an additional set of random numbers $\{q'\}$, uniformly distributed on the unit interval, was assigned to all bonds. The withdrawal thresholds $\varphi(q')$ for bond snap-off were then given by $\varphi(q')=-(q'+1)/2$ (analogous to the withdrawal thresholds for I2 site withdrawal). This modification again led to reduced withdrawal of the nonwetting fluid. Extensive bond fragmentation occurred if the ''pressure'' of the invading wetting fluid was equal to or greater than $-1/2$. In contrast to I2 site withdrawal, the withdrawal of bonds could not lead to untrapping of entire regions of wetting fluid. Consequently, the enhancement of the bond withdrawals did not expose further nonwetting fluid to withdrawal.

In a similar simulation in which the thresholds for both piston bond withdrawal and snap-off bond withdrawal was given simply by $\varphi(q')=-q'$, independent of the fluid topology, numerous snap-off withdrawals occurred, leading to extensive fragmentation at an early stage. Compared to the original model, snap-off bond withdrawal was much more favored. Extensive bond fragmentation occurred at an early stage, and very few sites were withdrawn.

More radical simplifications of the cluster fragmentation simulation model were also tested. In one version, the bonds were eliminated to reduce the model to a site IP model. The nonwetting fluid formed an IP cluster consisting of occupied sites, using a set of invasion thresholds assigned to the sites. The only two withdrawal mechanisms included in the model were I1 and I2 withdrawal steps, the distinction between the two being based on the state of the adjacent sites rather than on the state of adjacent bonds. In another simplified version, a bond IP model was used in which invasion thresholds and withdrawal thresholds were assigned to the bonds on a lattice of bonds. After the nonwetting fluid had formed an IP cluster consisting of occupied bonds, the nonwetting fluid was withdrawn using pistonlike bond withdrawals and snap-off bond withdrawals. None of the simplified models was found to reproduce the experimental displacement patterns in a satisfactory manner.

Versions of the site-bond IP model for cluster migration that were modified or simplified in manners analogous to those described above did not perform satisfactory. In the simulations discussed in the remainder of this text the site-bond IP models described in Secs. III B and III C were used.

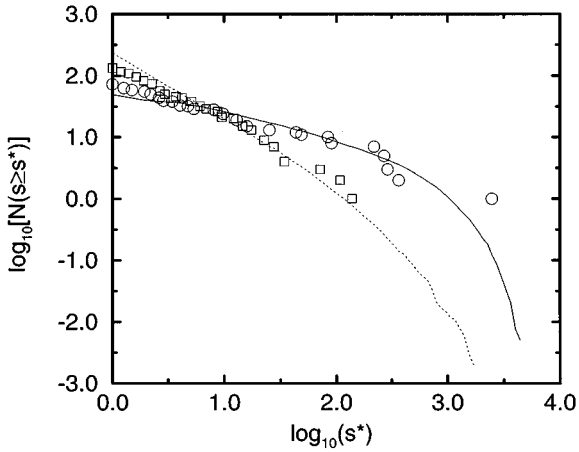

FIG. 12. Cumulative fragment size distributions $N(s\geqslant s^*)$ measured in the experiment shown in Fig. 2 (circles) and simulations (solid line) on IP cluster fragmentation at the final stage, plotted as a function of s^* on a log-log scale. s denotes the approximate number of occupied pores, and the number of occupied sites, respectively. Also shown are the cumulative size distributions $N(s\geqslant s^*)$ of trapped wetting fluid fragments, measured in the experiment (squares) and in simulations (dotted line).

IV. COMPARISON OF EXPERIMENTS AND SIMULATIONS

Quantitative comparisons of experiment and simulation were carried out by measuring the size distribution and scaling properties of the fragments. In the experiments, the size of a fluid fragment was determined by counting the number of pixels representing the fragment in the digitized image. One pore was represented by about 30 pixels. Fragments that occupied less than 30 pixels were ignored. Pixels belonging to a nonwetting fluid fragment were connected via nearest or next-nearest neighbors. Wetting fluid fragments were defined via nearest-neighbor connection of pixels. In the simulations, the size of a fragment was defined as the number of sites occupied by the fragment. The sites belonging to a fragment were connected via nearest-neighbor sites, linked by bonds.

A. Comparison between experiment and simulation on IP cluster fragmentation

Figure 12 shows, on a log-log plot, the cumulative distribution of nonwetting fluid fragments $N(s\geqslant s^*)$ vs s^*, measured in the experiment shown in Fig. 2(c). $N(s\geqslant s^*)$ denotes the number of fragments that have a size s equal to or greater than a size s^*. The distribution of fluid fragment sizes observed in simulations is also plotted in the same figure. The distribution of nonwetting fluid fragments was measured at the end of the simulations, when no more withdrawal was possible, and was averaged over several hundred simulations. The simulations were carried out on a lattice of 100×200 sites, corresponding to the cell size used in the experiment.

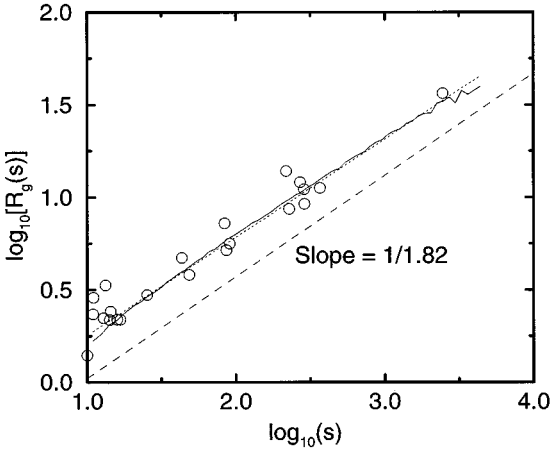

FIG. 13. The radius of gyration R_g of the nonwetting fluid fragments in experiments on IP cluster fragmentation, measured at the final stage and plotted as a function of fragment mass s. The circles refer to fragments observed in the pattern shown in Fig. 2(c), and the solid line refers to simulation data. The dotted line, with a slope of 0.53, is a linear least-squares fit to the simulation data. The dashed line has a slope of 0.55 corresponding to the inverse of the fractal dimensionality of IP clusters, with trapping.

Figure 12 also shows the cumulative size distribution of trapped wetting fluid clusters. The distribution was measured at the final stage in the experiment shown in Fig. 2 and in corresponding simulations. Only trapped wetting fluid clusters that were not adjacent to the edges of the experimental cell were taken into account.

The agreement between the fragment size distributions measured in the experiments and in the simulations is fair. Deviations are found in the distribution of trapped wetting fluid clusters. These may be attributed to the fact that a substantial part of the wetting fluid belonging to a trapped cluster was located in pore necks and channels (see Fig. 3). Fluid in channels connected to a cluster contributed to the total cluster size (mass). In the simulations, only wetting fluid sites contributed to the cluster size, leading to a potential underestimation of the size.

Figure 13 shows, on a log-log scale, the radius of gyration $R_g(s)$ of the nonwetting fluid fragments, plotted versus the fragment size s. $R_g(s)$ was measured at the final stage in edge-injection experiments and simulations. Only fragments with size $s>10$ were included. $R_g(s)$ was expected to scale with the fragment size s as [3]

$$R_g(s)\sim s^{1/D}, \tag{2}$$

where D is the fractal dimensionality of the fragments. If the fragments retain the structure of the original IP cluster, $R_g(s)\sim s^{1/1.82}\sim s^{0.55}$. Here, the fractal dimensionality $D\approx 1.82$ of IP clusters was inserted [2,25]. Both the simulation data and the experimental data are consistent with this assumption. A least-squares fit of the simulation data yielded $R_g(s)\sim s^{0.53}$.

B. Comparison between experiment and simulation on IP cluster migration and fragmentation

Each stage of a migration experiment was characterized by the ratio between the buoyancy and capillary forces acting, conveniently expressed by the modified Bond number $\mathrm{Bo}=(\Delta\rho g a^2/\sigma)\sin\alpha$, where a is a typical length scale describing the pore geometry of the medium. Using the values given in Sec. II and setting $a\approx$ 1 mm, Bo was found to vary from 0 to ≈ 0.04 when α was increased from 0° to about 10°. In the simulations, the quantity corresponding to Bo was the ratio $f/\langle\phi+\varphi\rangle$ between the buoyancy parameter f and a typical value for the sum of thresholds. The sum $\langle\phi+\varphi\rangle$ had a value of ≈ 0.5. The range of buoyancy drives investigated in the experiments was covered in most of the simulations by letting f vary from 0 to 0.02 in steps of 10^{-4}.

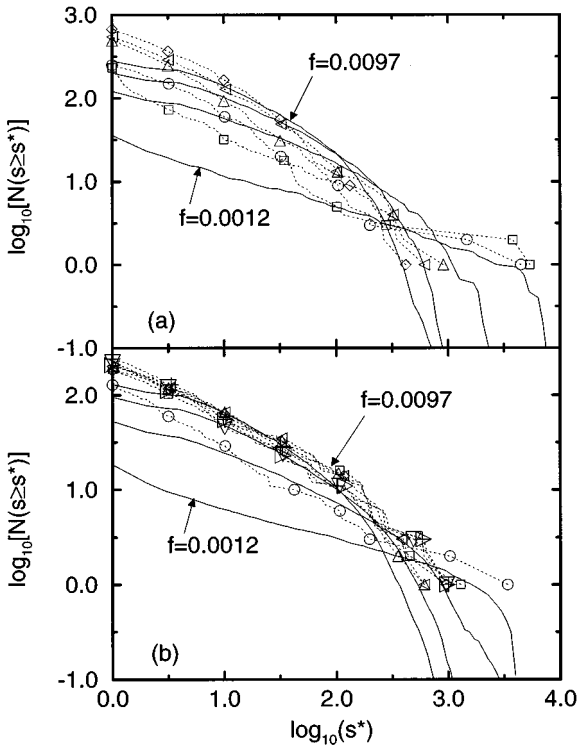

FIG. 14. Cumulative size distributions of nonwetting fluid fragments $N(s\geq s^*)$ observed in migration experiments (dotted lines and symbols), plotted as a function of s^* on a log-log scale. Different symbols refer to observations at different tilting angles α. The initial IP cluster covered about 4000 pores (a) and 8000 pores (b), respectively. The solid lines are the cumulative distributions observed in simulations.

Figure 14 shows a log-log plot of the cumulative size distribution $N(s\geq s^*)$ of fragments of the migrating IP cluster, measured in different experiments and simulations. The distributions were measured at various inclination angles α (experiments) and values of the buoyancy parameter f (simulations). In the experiments, the initial IP-like cluster of nonwetting fluid covered about 4000 and 8000 pores, respectively. The simulations were carried out using IP clusters of $s_0=4000$ and 8000 sites, respectively.

At each stage, the size distribution was measured when all migration had ceased. The agreement between the cluster fragment distributions found experimentally and measured in simulations is satisfying. The steep decay of the distributions at large s is not seen in the experimental data for statistical reasons.

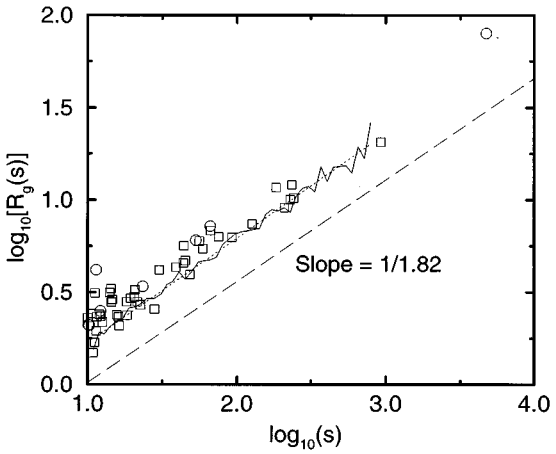

FIG. 15. The radius of gyration R_g of the nonwetting fluid fragments in experiments on IP cluster migration, measured at two slightly different tilting angles α (circles, squares). The solid line was obtained from measurements in simulations at a fixed value of the buoyancy parameter f. The dotted line, with a slope 0.57, is a linear least-squares fit to the simulation data. The dashed line has a slope of 0.55 corresponding to the inverse of the fractal dimensionality of IP clusters, with trapping.

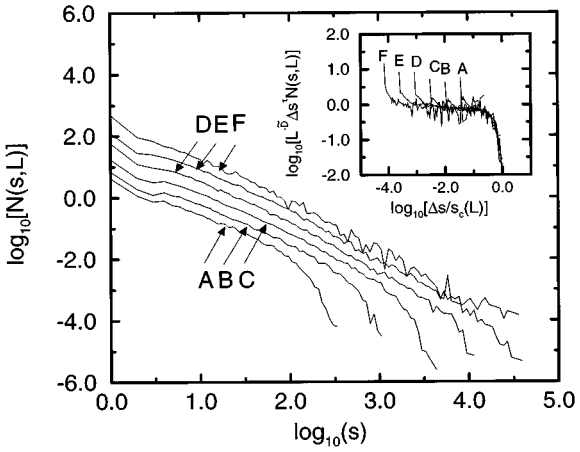

FIG. 16. The size distributions $N(s,L)$ of nonwetting fluid fragments measured in simulations of IP cluster fragmentation at the final stage, using lattices of size 25×50 (A), 50×100 (B), 100×200 (C), 200×400 (D), 400×800 (E), and 800×1600 (F), respectively. The inset shows an attempt to collapse the distributions, using the scaling form given in Eq. (3). The exponents τ and χ were obtained from an analysis of the moments $\mu^{(k)}$, assuming that $\tilde{D}=D+\chi(2-\tau)$. The cluster sizes were shifted to $\Delta s=s+10$.

As in Fig. 13, the radii of gyration R_g of the fragments observed in experiments and in simulations are plotted on a log-log scale as a function of the fragment size s in Fig. 15. The experimental data was measured at inclination angles of $\alpha=2.1°$ and 2.4°, respectively. The simulation data was measured at a buoyancy parameter of $f=0.0107$, using an initial IP cluster with $s_0=2000$ sites. A least-squares fit of the simulation data yielded $R_g(s)\sim s^{0.57}$. Both the experimental data and the simulation data are consistent with the idea that the fragments form small IP-like clusters with the fractal dimensionality of $D\approx1.82$.

V. SCALING PROPERTIES OF SELECTED QUANTITIES

In the experiments, the system size could not be varied over a large range due to practical limitations, and only a handful of experiments could be conducted. The scaling behavior of a number of quantities was studied by means of simulations. In the simulations of IP cluster fragmentation, the analysis included the study of the fragment size distributions and of the saturation with nonwetting fluid at the final stage. In the simulations of IP cluster migration and fragmentation, the dynamics of the migration process was studied by measuring and comparing properties of fragments that were immobile and of fragments that were in the process of migrating.

A. Results obtained in simulations of IP cluster fragmentation

Figure 16 shows the size distribution $N(s,L)$ of the nonwetting fluid fragments, measured on a log-log scale for simulations at the final stage. The simulation data of Fig. 12 is included in this figure. The data sets corresponding to the largest systems studied ($L=800$) appear noisy due to poor statistics. An attempt was made to represent the distributions by the scaling form [26]

$$N(s,L)\sim L^{\tilde{D}}\Delta s^{-\tau}g\left(\frac{\Delta s}{s_c(L)}\right). \tag{3}$$

Here, $\tilde{D}$ characterizes the dependence of the amount (mass) of nonwetting fluid remaining at the final stage on the system size L. $\Delta s=s+c$ is the fragment size, shifted by a constant amount c. The scaling function $g(x)$ is constant for $x\ll1$ and decays faster than any power of x for $x\gg1$. $s_c(L)$ represents the cutoff fragment size that was expected to scale with the system size as

$$s_c(L)\sim L^{\chi}. \tag{4}$$

The exponents τ and χ may be extracted from the scaling behavior of the moments of the fragment size distribution $N(s,L)$. The kth moment $\mu^{(k)}(L)$ of the distribution $N(s,L)$ is defined as

$$\mu_L^{(k)}=\sum_{s=0}^{\infty}s^kN(s,L). \tag{5}$$

For $L\gg1$ and $1<\tau<2$, the ratios of the moments were expected to scale with the system size as

$$\frac{\mu_L^{(1)}}{\mu_L^{(0)}}\sim L^{\chi(2-\tau)}$$

$$\frac{\mu_L^{(2)}}{\mu_L^{(1)}}\sim L^{\chi}. \tag{6}$$

Equation (6) was derived in a manner similar to the one described in Ref. [14]. Figure 17 shows a plot of these ratios as a function of the system size L. On a log-log scale, the ratios appeared to obey power laws, as expected. For the ratio of the first to the zeroth moment and for the ratio of the

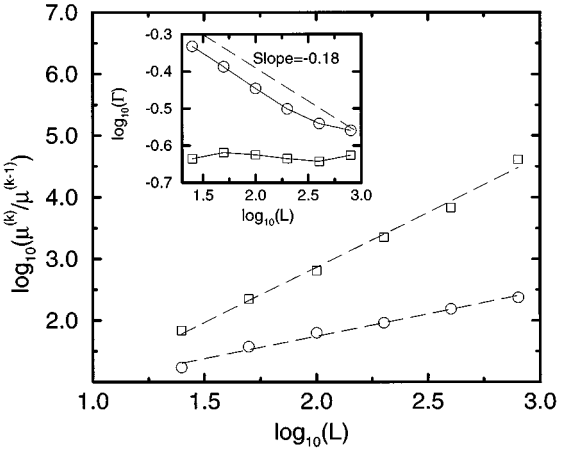

FIG. 17. Ratio $\mu^{(1)}/\mu^{(0)}$ (circles), and $\mu^{(2)}/\mu^{(1)}$ (squares), respectively, of moments $\mu_L^{(k)}$ of the fragment size distributions, measured at the final stage in simulations of IP cluster fragmentation and plotted on a log-log scale as a function of system size L. The dashed lines are linear least-squares fits. The inset shows the saturation Γ_b at breakthrough (points) and at the final stage Γ_f (squares), plotted versus L on a log-log scale. The dashed line indicates the scaling expected for IP clusters.

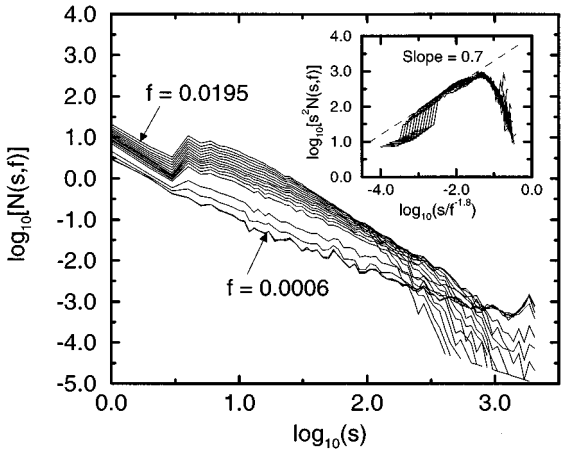

FIG. 18. Plot of the fragment size distribution $N(s,f)$ measured in simulations of IP cluster migration and fragmentation. The initial IP cluster had a size of $s_0=2000$ sites, and the buoyancy parameter f was increased in steps of size 0.0001 from 0 to 0.02. At low values of f, a peak at s_0 indicates incomplete fragmentation of the IP cluster. At high f, few large fragments remain. The insert shows an attempt to collapse the distributions onto a single scaling function $g(s/s_c)$, using the scaling form given in Eq. (8) with $s_c(f)\sim f^{-1.8}$. The distributions corresponding to the five lowest values of f were removed.

second to the first moment, linear least-squares fits yielded exponents of 0.73 ± 0.04 and 1.79 ± 0.08, respectively. Using Eq. (6), the exponents $\chi=1.79\pm0.08$ and $\tau=1.59\pm0.09$ were obtained.

The inset in Fig. 17 shows a plot of the breakthrough saturation Γ_b (the number of nonwetting fluid sites divided by the number of lattice sites at breakthrough). For IP clusters in two dimensions, the saturation scales as $\Gamma_b\sim L^{D-2}$ since the cluster size (mass) scales with the system size as $s\sim L^D$ [25]. The scaling of Γ_b with the system size L apparent in Fig. 17 is consistent with this expectation. During the withdrawal of the nonwetting fluid, Γ decreases from the breakthrough value to the final value Γ_f. The total amount of remaining nonwetting fluid may be expressed as the first moment of the fragment size distribution,

$$\Gamma_f(L)=L^{-2}\sum_{s=1}^{\infty} sN(s,L)=L^{-2}\mu_L^{(1)}. \tag{7}$$

The first moment of the fragment size distribution depends on the system size L as $\mu_L^{(1)}\sim L^{\tilde{D}+\chi(2-\tau)}$. The final saturation cannot scale with an exponent $\tilde{D}+\chi(2-\tau)-2$ greater than the IP exponent $D-2$, which leads to $\tilde{D}\leqslant D-\chi(2-\tau)$. In the inset in Fig. 17, Γ_f is plotted versus L on a log-log scale. The final saturation had a roughly constant value $\Gamma_f\approx0.23$ for all system sizes investigated, and does not appear to decay equally fast or faster than the breakthrough saturation Γ_b. This finding indicates that the asymptotic regime has not been reached in the simulations.

In the absence of a known value for the saturation exponent, it was assumed that $\tilde{D}$ has the maximum possible value $D-\chi(2-\tau)\approx1.09$. The inset in Fig. 16 shows the data collapse obtained using the scaling form given in Eq. (3) and the exponents τ and χ obtained from the analysis of the moments. The shift $\Delta s=s+10$ was chosen judiciously. The data collapse is very good. Using a shift of zero ($\Delta s=s$), the collapse is not impaired for large values of the scaling variable, but considerable spread was found for low values. From Fig. 16, it is apparent that the distributions $N(s,L)$ assume a power-law decay only for fragment sizes of the order of 10 and larger, up to the cutoff size $s_c(L)$. The transient behavior at very low s cannot be accounted for by the scaling function $g(x)$ and is remedied by the shift applied in Eq. (3).

B. Results obtained in simulations on IP cluster migration and fragmentation

In the simulations of IP cluster migration, the fragmentation depended on the buoyancy parameter f (corresponding to the effective acceleration of gravity $g\sin(\alpha)$ in the experiment). Fragments that were formed could disintegrate into smaller fragments or coalesce with other fragments during migration. The total amount of nonwetting fluid was held constant at all stages.

Figure 18 shows the fragment size distributions $N(s,f)$ measured on a log-log scale at different values of the gradient parameter f in simulations using initial IP clusters with a size $s_0=2000$. At low values of f, fragments of all sizes up to s_0 were present. The distribution of fragment sizes is peaked at values slightly below s_0, indicating that, in many runs of the simulation, the IP cluster was essentially intact at this stage. When f was increased, smaller fragments were formed at the expense of the large fragments. The distributions measured at high f are characterized by cutoff sizes $s_c(f)$ that decrease with increasing f.

A standard scaling form for fragment size distributions is [26]

$$N(s,f)\sim s^{-2}g\left(\frac{s}{s_c(f)}\right), \tag{8}$$

with the cutoff size s_c scaling with the parameter f as

$$s_c(f)\sim f^{-z}. \tag{9}$$

The insert in Fig. 18 shows the data collapse obtained by using the scaling form given in Eq. (8), using a value of 1.8 for the exponent z in Eq. (9). The distributions corresponding to the lowest values of f were omitted in the data collapse, since fragmentation and migration had not begun in all of the simulations at these stages. Equation (9) may be interpreted in terms of a simple picture in which the fragments are viewed as blobs with a IP clusterlike structure. In the simulations, the fragments that have a size close to the cutoff size $s_c(f)$ are characterized by an extension $l_c(f)$ in the y direction (the direction of the gradient imposed) that scales with f as

$$l_c(f)\sim f^{-1}, \tag{10}$$

as will be shown below. Assuming that the radius of gyration R_g of the fragments is proportional to the extension $l_c(f)$ and making use of Eq. (2), the relationship

$$s_c(f)\sim l_c^D(f)\sim f^{-D} \tag{11}$$

is obtained. Inserting the IP exponent $D\approx 1.82$, Eq. (11) is consistent with the empirical data collapse shown in Fig. 18.

Migration of both the initial IP cluster and the fragments that form begins when the buoyancy force acting on them become larger than the capillary forces. In the model, the capillary forces are represented by the quenched disorder with a magnitude of order unity and migration begins when $fl_y \gtrsim 1$, where l_y is the length of the cluster in the y direction. Consequently, a characteristic length $l_y^{(m)}(f)\sim f^{-1}$ in the y direction can be defined for each value of the buoyancy parameter f. Clusters that extend over distances greater than $\approx l_y^{(m)}(f)$ in the y will migrate under the influence of the buoyancy forces, and clusters that extend over distances less than $\approx l_y^{(m)}(f)$ in the y direction will be trapped in the porous medium by the capillary forces. Figure 19(a) shows a scatter plot of the y extensions $l_y^{(m)}$ of fragments that began a sequence of migration steps at a gradient f, on a log-log scale. The mean extension $\overline{l_y^{(m)}(f)}=\Sigma(l_y^{(m)}(s))^2N(s)/\Sigma l_y^{(m)}(s)N(s)$ scales as $\overline{l_y^{(m)}(f)}\sim f^{-1}$ in the migration regime, where $f>f_c(s_0)$. At the onset of migration, most of the fragments were not elongated in the y direction. The size $s^{(m)}$ of these fragments then may be expected to scale with the buoyancy parameter as

$$s^{(m)}(f)\sim f^{-D}, \tag{12}$$

where $D\approx 1.82$ is the fractal dimensionality of IP clusters.

During a typical sequence of migration steps, the extension of the fragment in the y direction increased up to a value of about $l_y^{(p)}$, leading to a further increase in the buoyancy force. Some of the steps led to the formation of fragments that were left behind, as the larger part of the fragmented cluster continued to migrate. The migrating fragments were elongated in the y direction.

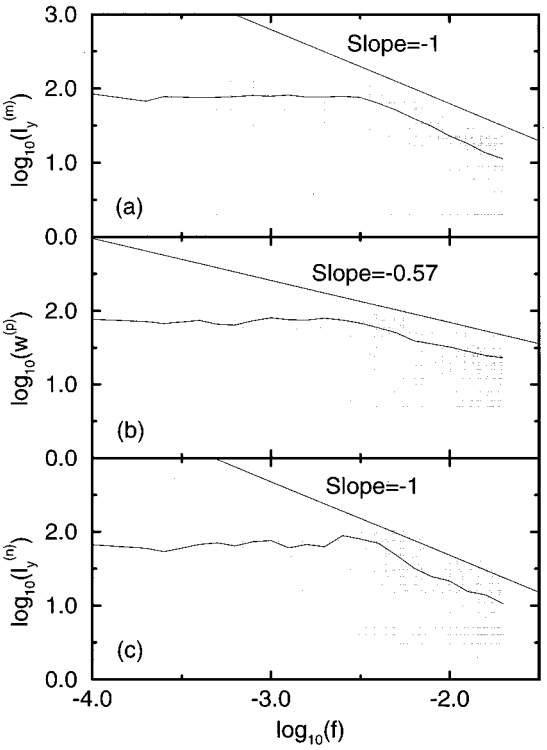

FIG. 19. Scatter plots of fragment extensions vs the gradient parameter f on a log-log scale. Part (a) shows the extension in the y direction $l_y^{(m)}$ of fragments that started to migrate. Part (b) shows the width $w^{(p)}$ of fragments that were in the process of migrating, at stages before they underwent fragmentation. Part (c) shows the extension in the y direction $l_y^{(n)}$ of fragments that were newly formed. The initial IP clusters had a size of $s_0=2000$ sites. The solid lines indicate averages.

Figure 19(b) shows on a log-log scale a scatter plot of the width $w^{(p)}$ of migrating fragments, at stages before they underwent fragmentation, as a function of the gradient f. The plot is consistent with the idea that the width is a measure for the percolation correlation length ξ characterizing the structure of nonwetting fluid. In the presence of a gradient f, the correlation length is known to scale as [27]

$$\xi\sim|f|^{-\nu/(\nu+1)} \tag{13}$$

with $\nu/(\nu+1)\approx 0.57$.

The migration of a typical fragment of size $s^{(m)}(f)$ ceased when the y extension of the fragment dropped below the characteristic length $l_y^{(m)}(f)$, after a sequence of fragmentation processes. The remaining part of the migrating fragment had a size $s'<s^{(m)}(f)$, and was not elongated in the y direction. Similarly, the fragments formed during the sequence were not elongated in the y direction. The typical extension in the y direction of fragments formed at a buoyancy parameter of f was found to scale as $l_y^{(n)}(f)\sim f^{-1}$ as shown in Fig. 19(c). The typical size of fragments formed during migration at f may then again be expected to scale as

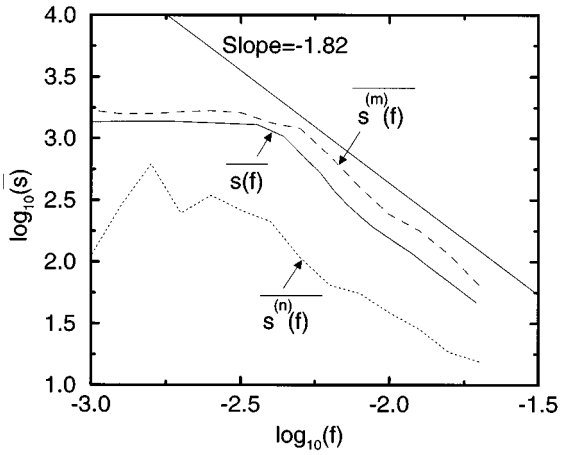

FIG. 20. The mean fragment size $\overline{s(f)}$ (solid line) was bounded by the mean size $\overline{s^n(f)}$ of fragments that were newly formed at a given f (dotted line), and by the mean size $\overline{s^m(f)}$ of fragments that started to migrate at a given f (dashed line), respectively. The initial IP clusters had a size of $s_0=2000$ sites. The expected scaling behavior is indicated (straight solid line).

$$s^{(n)}(f)\sim f^{-D}. \tag{14}$$

Figure 20 shows the mean fragment size $\overline{s(f)}=\Sigma s^2 N_s(f)/\Sigma s N_s(f)$ plotted as a function of the buoyancy parameter f on a log-log plot. Also shown is the mean size $\overline{s^{(m)}(f)}$ of fragments that started to migrate at a given stage, and the mean size $\overline{s^{(n)}(f)}$ of fragments that were newly formed at a given stage. The data are consistent with the scaling laws given in Eqs. (12) and (14).

VI. CONCLUSIONS

In the experiments described in this paper, IP-like clusters of a nonwetting fluid embedded in a wetting fluid were fragmented in a porous medium. In the experiments on IP cluster fragmentation, the fragmentation of the cluster occurred by removing parts of the cluster. The internal structure of the fragments was not changed. In the experiments on IP cluster migration and fragmentation, the cluster fragments were deformed in the course of the experiment. The fragments formed in these experiments not only depended on the sequence of invasion and withdrawal events imposed by the pore geometries but also on the migration dynamics.

The main results emerging from the present study are as follows: (i) The experiments were simulated using modified site-bond IP models, and good agreement was found between the simulations and experiments. Emphasis was placed on modeling a hierarchy of possible displacement events: pistonlike withdrawal of wetting fluid from bonds, type-I1 withdrawal from sites, type-I2 withdrawal from sites, and snap-off withdrawal from bonds. A similar ordering of displacement mechanisms was used in simulation models introduced by Blunt, King, and Scher [28] and Glass and Yarrington [29]. The success of the simulation model indicates that IP models are well suited to model slow two-phase fluid flow with complex boundary conditions, despite the fact that the model does not contain a detailed representation of the various displacement mechanisms found in real porous media with complex geometries and wetting behavior.

(ii) In both types of experiments and simulations, a fractal fluid cluster underwent fragmentation. The resulting irregular fragments could be described by the same fractal dimensionality $D\approx 1.82$ as the initial cluster. This dimensionality is characteristic for an invasion percolationlike structure (embedded in two dimensions, with a trapping rule). The fragmentation and migration processes led to constant changes of the displacement patterns at global and local scales, but did not change the internal arrangement of the fragmenting structure.

(iii) The distributions of fragment sizes measured in simulations could be represented by simple scaling forms and characterized by typical (cutoff) sizes. In the cluster fragmentation process, the cutoff size had a power-law dependence on the system size L, with an exponent χ very close and possibly equal to D. In the cluster migration process the cutoff size of the distributions was given by the magnitude of the gradient f driving the process, for f sufficiently large. In this regime the cutoff size had a power-law dependence on f, with the exponent D.

ACKNOWLEDGMENTS

We thank A. Aharony, K. Christensen, V. Frette, L. Furuberg, P. King, R. Lenormand, and K. J. Måløy for helpful discussions. We acknowledge support by VISTA, a research cooperation between The Norwegian Academy of Science and Letters and Den norske stats oljeselskap a.s. (STATOIL) and by The Research Council of Norway (NFR). This research has received support from the NFR program for supercomputing through a grant of computing time.

[1] J. Feder, *Fractals* (Plenum, New York, 1988).
[2] R. Lenormand and C. Zarcone, Phys. Rev. Lett. **54**, 2226 (1985).
[3] D. Stauffer and A. Aharony, *Introduction to Percolation Theory*, 2nd ed. (Taylor & Francis, London, 1992).
[4] P. G. de Gennes and E. Guyon, J. Méc. **17**, 403 (1978).
[5] R. G. Larson, L. E. Scriven, and H. T. Davis, Chem. Eng. Sci. **36**, 57 (1981).
[6] D. Wilkinson, Phys. Rev. A **34**, 1380 (1986).
[7] J. P. Hulin, E. Clément, C. Baudet, J. F. Gouyet, and M. Rosso, Phys. Rev. Lett. **61**, 333 (1988).
[8] M. Rubio, C. Edwards, A. Dougherty, and J. Gollub, Phys. Rev. Lett. **63**, 1685 (1989).
[9] B. Albert-László, S. V. Buldyrev, S. Havlin, G. Huber, H. E. Stanley, and T. Vicsek, in *Surface Disordering: Growth, Roughening and Phase Transitions*, edited by R. Jullien, J. Kertész, P. Meakin, and D. E. Wolf (Nova Science, New York, 1992).
[10] G. Wagner, A. Birovljev, P. Meakin, J. Feder, and T. Jøssang, Europhys. Lett. **31**, 139 (1995).

[11] A. Birovljev, G. Wagner, P. Meakin, J. Feder, and T. Jøssang, Phys. Rev. E **51**, 5911 (1995).
[12] D. Wilkinson and J. F. Willemsen, J. Phys. A **16**, 3365 (1983); R. Lenormand and S. Bories, C.R. Acad. Sci. Paris **291**, 279 (1980); R. Chandler, J. Koplik, K. Lerman, and J. F. Willemsen, J. Fluid Mech. **119**, 249 (1982).
[13] M. A. F. Gomes and G. L. Vasconcelos, J. Phys. A **22**, L757 (1989); M. A. F. Gomes and G. L. Vasconcelos, Comput. Phys. Commun. **54**, 257 (1989).
[14] M. F. Gyure and B. F. Edwards, Phys. Rev. Lett. **68**, 2692 (1992); B. F. Edwards, M. F. Gyure, and M. V. Ferer, Phys. Rev. A **46**, 6252 (1992); M. F. Gyure, M. V. Ferer, B. F. Edwards, and G. Huber, Phys. Rev. E **51**, 2632 (1995).
[15] J.-F. Gouyet, Phys. Rev. B **47**, 5446 (1993).
[16] C. Mattax and J. Kyte, Oil Gas J. **59**, 115 (1961); A. Chatenver, M. K. Indra, and J. R. Kyte, J. Petr. Tech. **11**, 13 (1959).
[17] R. Lenormand and C. Zarcone (unpublished); R. Lenormand, J. Phys. Condens. Matter **2**, SA79 (1990).
[18] N. C. Wardlaw and R. P. Taylor, Bull. Can. Pet. Tech. **24**, 225 (1976).
[19] R. Lenormand, C. Zarcone, and A. Sarr, J. Fluid Mech. **135**, 337 (1983).
[20] J. S. Buckley, in *Interfacial Phenomena in Petroleum Recovery*, edited by N. R. Morrow (Marcel Dekker, New York, 1991), pp. 157–189.
[21] J.-D. Chen and J. Koplik, J. Colloid Interface Sci. **108**, 304 (1985).
[22] W. B. Haines, J. Agri. Sci. **20**, 97 (1930); K. J. Måløy, L. Furuberg, J. Feder, and T. Jøssang, Phys. Rev. Lett. **68**, 2161 (1992).
[23] Y. Li and N. C. Wardlaw, J. Colloid Interface Sci. **109**, 473 (1986).
[24] N. C. Wardlaw and Y. Li, Transp. Porous Media **3**, 17 (1988).
[25] L. Furuberg, J. Feder, A. Aharony, and T. Jøssang, Phys. Rev. Lett. **61**, 2117 (1988).
[26] T. Vicsek and F. Family, Phys. Rev. Lett **52**, 1669 (1984).
[27] D. Wilkinson, Phys. Rev. A **30**, 520 (1984).
[28] M. Blunt, M. J. King, and H. Scher, Phys. Rev. A **46**, 7680 (1992); M. J. Blunt and H. Scher, Phys. Rev. E **52**, 6387 (1995).
[29] R. J. Glass and L. Yarrington, Geoderma **70**, 231 (1996).